NMR Experiments Reveal Distinct Antibody-Bound Conformations of a Synthetic Disaccharide Representing a General Structural Element of Bacterial Lipopolysaccharide Epitopes†

Thomas Haselhorst,‡ Juan-Felix Espinosa,§ Jesus Jiménez-Barbero,§ Tobias Sokolowski,‡ Paul Kosma,|| Helmut Brade,⊥ Lore Brade,⊥ and Thomas Peters*,‡

Institut für Chemie, Medizinische Universität Lübeck, Ratzeburger Allee 160, D-23538 Lübeck, Germany, Instituto de Química Orgánica General, CSIC, Juan de la Cierva 3, E-28006 Madrid, Spain, Institut für Chemie der Universität für Bodenkultur Wien, A-1190 Wien, Austria, and Forschungszentrum Borstel, Zentrum für Medizin und Biowissenschaften, Parkallee 22, D-23845 Borstel, Germany

Received December 18, 1998; Revised Manuscript Received March 16, 1999

ABSTRACT: The recognition reactions between a synthetic disaccharide α-Kdo-(2→4)-α-Kdo-(2→O)-allyl and two monoclonal antibodies (mAbs) were studied by NMR, yielding two distinct bound conformations of the carbohydrate ligand. One mAb, S23-24, recognizes the disaccharides α-Kdo-(2→4)-α-Kdo-(2→O)-allyl and α-Kdo-(2→8)-α-Kdo-(2→O)-allyl with similar affinities, whereas mAb S25-2 binds to the disaccharide α-Kdo-(2→8)-α-Kdo-(2→O)-allyl with an approximately 10-fold higher affinity than to the disaccharide α-Kdo-(2→4)-α-Kdo-(2→O)-allyl. Compared to S25-2, S23-24 binds to α-Kdo-(2→4)-α-Kdo-(2→O)-allyl with an approximately 50-fold increased affinity. We used NMR experiments that are based on the transferred NOE effect, specifically, trNOESY, trROESY, QUIET-trNOESY, and MINSY experiments, to show that the (2→8)-specific mAb, S25-2, stabilizes a conformation of the α-(2→4)-linked disaccharide that is not highly populated in solution. S23-24 recognizes two conformations of α-Kdo-(2→4)-α-Kdo-(2→O)-allyl, one that is highly populated in aqueous solution and another conformation that is similar to the one bound by S25-2. This is the first example where it is experimentally shown that a carbohydrate ligand may adopt different bioactive conformations upon interaction with mAbs with different fine specificities. Our NMR studies indicate that a careful examination of spin diffusion is critical for the analysis of bioactive conformations of carbohydrate ligands.

Although it is well established that carbohydrate−protein interactions are generally important in biology, there are still many open questions, especially concerning the understanding of the molecular level of such interactions. The main tools that furnish experimental data at atomic resolution are X-ray structural analysis and NMR spectroscopy. In cases where protein−ligand interactions are weak, trNOE[1] experiments have emerged as an important technique for deriving bioactive conformations of ligand molecules (*1*−*3*). Therefore, carbohydrate-protein complexes are an ideal target for trNOE studies (*4*, *5*). Recently, we reported that trNOE experiments are even useful for screening compound libraries for biological activity (*6*−*8*). In most cases reported so far, proteins recognize carbohydrate conformations that represent either the global energy minimum or one of the major solution conformers. Exceptions have been identified only recently. In one case, a high-energy conformation of C-lactose, a nonhydrolyzable substrate analogue of *Escherichia coli β*-galactosidase, was identified as the enzyme-bound conformation (*9*). In a second case, a high-energy conformation of a glycosidic linkage in an antibody-bound *Salmonella*-type pentasaccharide was observed (*10*). A hexose residue flanking the binding pocket was found to adopt the anti conformation in the bound state. The trisaccharide portion of the pentasaccharide that lies inside the binding pocket was nearly undisturbed as has been described in a previous combined crystallographic and NMR study (*11*). Another trNOE study with the antibody-bound conformation of a *Streptococcus* group A trisaccharide revealed that a local minimum of the hapten that is also populated in aqueous solution is recognized by the protein (*12*).

Recently, we investigated the binding of the synthetic disaccharide α-Kdo-(2→8)-α-Kdo-(2→O)-allyl **2** to a mAb, S25-2 (*13*). The monosaccharide component 3-deoxy-D-*manno*-oct-2-ulosonic acid (Kdo) is an essential component

† This work was financially supported by grants from the Deutsche Forschungsgemeinschaft DFG (SFB470, Projects B3 and C1), from the Fonds der Chemischen Industrie (VCI), and from the Bundesministerium für Bildung und Forschung BMBF (BMBF 0311361). We acknowledge continuing support from Bruker Analytik GmbH (Rheinstetten, Germany). J.-F.E. was supported by a fellowship of the Spanish Ministerio de Education y Cultura.

* To whom correspondence should be addressed. Phone: +49-451-500-4230. Fax: +49-451-500-4241. E-mail: thomas.peters@chemie.muluebeck.de.

‡ Medizinische Universität Lübeck.

§ CSIC.

|| Institut für Chemie der Universität für Bodenkultur Wien.

⊥ Zentrum für Medizin und Biowissenschaften.

[1] Abbreviations: Kdo, 3-deoxy-d-*manno*-oct-2-ulosonic acid; LPS, lipopolysaccharide; MINSY, mixing irradiation during NOESY; MMC, Metropolis Monte Carlo; QUIET-NOESY, quenching undesirable indirect external trouble in nuclear Overhauser effect spectroscopy; ROESY, rotating frame NOESY; trNOE, transferred nuclear Overhauser effect.

10.1021/bi982984z CCC: $18.00
Published on Web 04/24/1999

of the LPS of Gram-negative bacteria (*14*). Whereas the disaccharide α-Kdo-(2→4)-α-Kdo constitutes a common structural element of the core region of Gram-negative bacterial LPS in general, the trisaccharide α-Kdo-(2→8)-α-Kdo-(2→4)-α-Kdo is a genus-specific epitope of the lipopolysaccharide of the obligate intracellular human pathogen *Chlamydia* (*15*). These parasites are responsible for a variety of diseases in animals and humans. During infection, antibodies are expressed against components in the outer membrane, with LPS as one of the major surface antigens. Several mAbs were raised against distinct epitopes of the carbohydrate moiety of chlamydial LPS (*16*). Two of these mAbs, S25-2 and S23-24, are studied in the work presented here.

A major problem for the analysis of the conformation of α-Kdo-(2→8)-α-Kdo-(2→O)-allyl **2** bound to S25-2 was the extensive overlap of almost all ^{1}H NMR signals of **2**, indicating the limits of the method. Nevertheless, we were able to define a range of possible bound conformations showing that the antibody probably binds to a conformer that is significantly populated in aqueous solution and that may be similar to the conformation found in the crystalline state of α-Kdo-(2→8)-α-Kdo-(2→O)-allyl **2** (*17*). In this study, we extend this work to the binding reactions of the related disaccharide α-Kdo-(2→4)-α-Kdo-(2→O)-allyl **1** to two distinct antibodies, S25-2 and S23-24, addressing the question of how different antibodies recognize a particular carbohydrate ligand.

MATERIALS AND METHODS

Serology. The generation of the mAb's (IgG_1 type) used in this study and their purification by affinity chromatography have been described (*16*). Binding of mAbs to their ligands was tested by EIA using synthetic neoglycoconjugates containing as a ligand the disaccharides α-Kdo-(2→4)-α-Kdo **1** or α-Kdo-(2→8)-α-Kdo **2**, which were synthesized as allyl glycosides, condensed with cysteamine, activated with thiophosphate, and coupled to BSA as described previously (*18*). Details of the assay have been described elsewhere (*19*).

Sample Preparation. First, 3.6 mg (6.07 μmol) of synthetic (*18*) α-Kdo-(2→4)-α-Kdo-(2→O)-allyl **1** (dipotassium salt, monohydrate, molecular mass of 597.60 Da) was lyophilized twice from 1.0 mL of D_2O (99.9 at. % D) and was then dissolved in 500 μL of D_2O (99.998 at. % D). mAb S23-24 was transferred into a 10 mM deuterated acetate buffer (d_3-acetic acid/d_3-sodium acetate, 99.9 at. % D, adjusted to pH 4.0) using Centricon filters (excluding molecular mass of 30 kDa; Amicon). The protein concentration was determined with the Lowry test (purchased from Sigma) (*20*) using bovine IgG as a standard. In a series of control transfer NOESY experiments, the molar ratio of mAb binding sites to carbohydrate ligand was increased up to 1:20, and ratios between 1:10 and 1:15 were found to yield optimum trNOEs. Two final samples were prepared, one containing 22 nmol (44 nmol of binding sites) of mAb S23-24 and 346 μg (583 nmol) of ligand in 610 μL of buffer, corresponding to an mAb binding site concentration of 72 μM and a ligand concentration of 0.955 mM (molar ratio of 1:13). The other sample contained 40 nmol (80 nmol of binding sites) of mAb S23-24 and 463 μg (781 nmol) of ligand in 600 μL of buffer, corresponding to an mAb binding site concentration of 133 μM and a ligand concentration of 1.301 mM (molar ratio of 1:10). The exchangeable protons of mAb S25-2 were exchanged against deuterium using D_2O by repeated cycles of freeze-drying and dissolving. A sample of the mAb−carbohydrate complex was prepared containing 5.0 mg (33.3 nmol, 66.6 nmol of binding sites) of mAb S25-2 in PBS buffer [10 mM phosphate and 10 mM NaCl (pH 6.0)] and 382 μg (644 nmol) of α-Kdo-(2→4)-α-Kdo-(2→O)-allyl disaccharide **1**, leading to a final concentration of 121 μM for the mAb binding sites and of 1.17 mM for disaccharide **1**. This corresponds to a molar ratio of 1:10 of mAb binding sites to carbohydrate ligand.

NMR Experiments. All NMR experiments were performed on a Bruker Avance DRX500 spectrometer (Institute for Chemistry, Medical University of Lübeck) operating at a proton frequency of 500.13 MHz. The measurements were performed at 310 K without sample spinning using the HDO signal as an internal reference (4.65 ppm at 310 K). Data acquisition and processing were performed with XWINNMR software (Bruker) running on Silicon Graphics Indy workstations. trNOEs were integrated with the program AURELIA (Bruker).

Chemical shifts and coupling constants for **1** were derived from a first-order analysis of the ^{1}H NMR spectra that were treated with a Lorentz−Gauss function prior to Fourier transformation. For the analysis of coupling constants between the protons H7, H8*pro-R*, and H8*pro-S* in pyranose ring b, a higher-order analysis was performed using the program GNMR, version 3.6.5 (Cherwell Scientific).

Two-dimensional (2D) NOESY experiments with free **1** were performed using TPPI (*21*). A total of 512 (t_1) × 2K (t_2) data points were recorded. Thirty-two scans and 16 dummy scans were performed. The relaxation delay was set at 3.8 s, and a value of 900 ms was chosen for the mixing time. Suppression of the residual HDO signal was achieved by presaturation with a weak rf field for 1 s during the relaxation delay and during the mixing time.

To remove Hartmann−Hahn artifacts, 2D ROESY and 2D trROESY experiments were performed as T-ROESY experiments (*22*) with a phase-alternated 180° pulse to generate the spin-lock field. A total of 2K (t_2) × 512 (t_1) data points were recorded. The carrier frequency of the spin-lock field was set at 2.89 ppm to further attenuate Hartmann−Hahn transfer. The spin-lock field had a width of 2.65 kHz. The mixing times in the trROESY experiments were 150, 250, and 350 ms. ROESY experiments for the free ligand were obtained with a mixing time of 350 ms (data not shown). Thirty-two scans were performed per t_1 increment with 32 dummy scans at the beginning in each case. The HDO signal was suppressed by presaturation for 1 s during the relaxation delay. The total relaxation delay was 3.5 s. Prior to Fourier transformation, the data matrix was zero-filled to yield a 2K × 1K data matrix that was multiplied with a 90° phase-shifted squared sine-bell function in both dimensions. A spectral width of 10 ppm was used in both dimensions.

2D trNOESY spectra were recorded with 512 increments in t_1 and 2K data points in t_2. The spectral width was 10 ppm in both dimensions. A spin-lock pulse with a strength of 5 kHz and a duration of 10 ms was applied after the first 90° pulse to suppress protein ^{1}H NMR signals (*23*). After 64 dummy scans, 32 scans were performed per t_1 increment. The residual HDO signal was presaturated with a weak rf field during relaxation and mixing time. A gradient pulse (1

ms, 5 G/cm) at the end of the mixing time was applied to remove transverse magnetization and thus to improve the quality of the spectra. Mixing times of 80, 150, 250, 350, 450, and 600 ms were chosen to generate NOE buildup curves.

2D QUIET-trNOESY spectra (*24*) were recorded with a modified NOESY sequence. After the first 90° pulse, the protein signals were suppressed by a spin-lock field (5 kHz, 10 ms). In the middle of the mixing time, a Gaussian Q3 cascade (*25*) was used for double-selective inversion. The programs xShape and Mule (Bruker) were used to generate multiple selective pulse shapes. In general, the truncation level was 1% and 256 data points were used. One QUIET-trNOESY experiment was performed with a triple-selective inversion pulse with a duration of 35 ms. The inversion pulses were calibrated by adjusting to maximum intensity the inverted region with a modified one-dimensional (1D) QUIET-trNOESY pulse sequence. A gradient pulse (1 ms, 5 G/cm) at the end of the mixing time was used to improve the spectra quality. A total of 512 × 2K data points were recorded, zero filled to 1K × 2K, and multiplied with a 90° phase-shifted squared sine-bell functions prior to Fourier transformation. The spectral width was 10 ppm in F_1 and F_2. After 64 dummy scans, 32 scans were performed per t_1 increment. The residual HDO signal was presaturated with a weak rf field during the relaxation time. The mixing times were 80, 150, 250, 350, 450, and 600 ms.

For the protein−carbohydrate complex, transient NOE experiments with continuos wave irradiation during the mixing time (MINSY) (*26*) were recorded. The spectral width was 15 ppm. A total of 16K data points were acquired, and prior to Fourier transformation, the FIDs were apodized by exponential multiplication. Four dummy scans and 8K scans are acquired. The total relaxation delay was set to 2.1 s. A 180° Gaussian pulse with a duration of 80 ms was employed for selective inversion of H3ax^c. The protons H6^b and H3eq^c were saturated by low-power rf irradiation during the 200 ms mixing time. For the selective inversion of H3eq^c, protons H6^b and H3ax^c were saturated during the 200 ms mixing time. Zero-filling of the acquired data (512 t_1 values and 2K data points in t_2) led to a final data matrix of 1K × 2K ($F_1 \times F_2$) data points. The baseline was corrected in F_2 and F_1 (third-order polynomial) prior to integration of cross-peak volumes. Volume determinations and the calculation of initial slopes were performed with the program AURELIA (*27*).

Spectra were processed with XWINNMR (Bruker) software. Experimental NOE curves were fitted to double-exponential function $f(t) = p0 \times \exp(-p2 \times t)[1 - \exp(-p1 \times t)]$, with $p0-p2$ being adjustable parameters. The initial slope was determined from the first derivative at time zero [$f'(0) = p0 \times p1$]. From the initial slopes, interproton distances r were obtained employing the isolated spin pair approximation. The distance r between protons H4^c and H6^c is independent of the glycosidic linkage conformation and was used as a reference ($r = 2.45$ Å) (*17*). For the calculation of absolute NOEs (Figure 6), the decay curves of the diagonal signals of H4^c and H3eq^b were fitted to an exponential function with the form $f(\tau_m) = C \times \exp(\tau_m/T_{1sel})$, where C is the scaling factor, τ_m is the mixing time, and T_{1sel} is the selective spin−lattice relaxation time for extrapolating to a mixing time τ_m of 0 ms. The volume of the diagonal signal at mixing time zero is defined as 100%, and absolute NOEs are given in percentages.

Table 1: ^{1}H Chemical Shifts δ (Parts per Million) of α-Kdo-(2→4)-α-Kdo-(2→O)-allyl **1** in D_2O at 310 K and 500.13 MHz

	unit b, α-Kdo-(2→4	unit c, α-Kdo-(2→O
H3ax	1.87	2.02
H3eq	2.24	2.10
H4	4.18	4.24
H5	4.14	4.18
H6	3.71	3.65
H7	4.08	4.04
H8*pro-R*	3.84	3.71
H8*pro-S*	4.07	4.02

Low-energy conformations and energy surfaces were calculated using the GEGOP program (*28*). Dihedral angles ϕ and ψ at the glycosidic linkages, and ω at the C5−C6 bonds, were defined as follows: ϕ = C1′−C2′−Ox−Cx, ψ = C2′−O2′−Cx−Hx, ω_1 = C8−C7−C6−C5, and ω_2 = O8−C8−C7−C6, with x being the aglyconic linkage site. Glycosidic bond angles were fixed at 117°, and pyranose rings were treated as rigid units in the $^5C_2$ conformation. Coordinates were taken from the X-ray structure (*17*). MMC simulations (*29*, *30*) were carried out on a Silicon Graphics O2 R10000 workstation with 2 × 10^6 macro steps each and temperature parameters set at 600 and 2000 K (*13*, *31*).

The bound conformation of α-Kdo-(2→4)-α-Kdo-(2→O)-allyl **1** was deduced as follows. First, interproton distances were obtained from experimental trNOE curves using the distance between protons H4^c and H6^c as a reference (see above). To derive upper and lower bounds for the distance constraints, an experimental error of ±20% was assumed and added to the distances. The ensemble of conformations obtained from a MMC simulation at 2000 K was then explored for those conformers that fulfilled the constraints. To further verify the analysis of bound conformations, interglycosidic trNOEs that were not observed were translated into negative distance constraints, with a corresponding minimum distance of 3.5 Å. All constraints are summarized in Table 3.

Theoretical ensemble average NOEs were calculated from $\langle r^{-6} \rangle$ averaged relaxation matrixes as has been described in detail previously (*32*). Theoretical ensemble-averaged NOEs were then calculated for a mixing time of 900 ms. A correlation time of 150 ps was chosen (*13*).

RESULTS AND DISCUSSION

Conformational Analysis of α*-Kdo-(2→4)-*α*-Kdo-(2→O)-allyl **1***. In contrast to the (2→8)-linked disaccharide **2** (*13*), disaccharide **1** exhibits several ^{1}H NMR signals that are well-separated and allow a variety of NMR experiments. A complete assignment of ^{1}H NMR resonance signals was achieved on the basis of COSY, TOCSY, and NOESY experiments (Table 1). Chemical shifts and coupling constants of **1** were in accordance with the values reported previously (*33*) and are summarized in Tables 1 and 2. Analysis of the side chain orientations of pyranose rings b and c in **1** requires the stereospecific assignment of protons H8*pro-R*^{b,c} and H8*pro-S*^{b,c}. This is of particular importance for unit b, because protons H8*pro-R*^{b} and H8*pro-S*^{b} are involved in interglycosidic NOE contacts. The stereospecific assignment for unit b is straightforward. Since the vicinal coupling constant ^3J(H6^b,H7^b) is 8.2 Hz, only a trans

Table 2: First-Order Coupling Constants $^3J_{(H,H)}$ (Hertz) of α-Kdo-(2→4)-α-Kdo-(2→O)-allyl **1** in D_2O at 310 K and 500.13 MHz[a]

	unit b, α-Kdo-(2→4	unit c, α-Kdo-(2→O
H3ax−H3eq	−13	−12.8
H3ax−H4	12.3	11.8
H3eq−H4	4.6	5.1
H4−H5	2.8	2.8
H5−H6	≅0	≅0
H6−H7	8.2	8.5
H7−H8*pro-R*	7.8 (7.5)	nd
H7−H8*pro-S*	3.5 (3.5)	nd
H8*pro-R*−H8*pro-S*	−12.5 (−12.5)	nd

[a] nd, not determined. Higher-order coupling constants from GNMR simulations are given in parentheses.

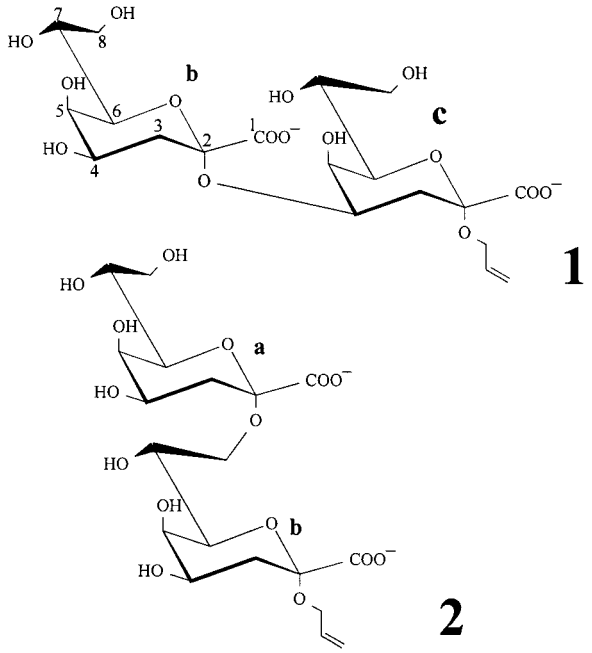

FIGURE 1: Disaccharides α-Kdo-(2→4)-α-Kdo-(2→O)-allyl **1** and α-Kdo-(2→8)-α-Kdo-(2→O)-allyl **2**.

orientation of the corresponding protons $H6^b$ and $H7^b$ is possible. Interglycosidic NOEs are observed from protons attached both to $C8^b$ to $H4^c$ and to protons $H3eq^c$ and $H3ax^c$. Due to the trans orientation of the protons attached to the $C6^b-C7^b$ bond, only one assignment for protons $H8pro\text{-}R^b$ and $H8pro\text{-}S^b$ is in accordance with both the interglycosidic NOEs and the coupling constants around the $C7^b-C8^b$ bond (cf. Figure 7 for three-dimensional images of **1**). From a higher-order analysis of the ^1H NMR spectrum using the program GNMR, the following coupling constants were obtained (cf. Table 2): $^3J(H7^b,H8pro\text{-}R^b) = 7.5$ Hz, $^3J(H7^b,H8pro\text{-}S^b) = 3.5$ Hz, and $^2J(H8pro\text{-}R^b,H8pro\text{-}S^b) = -12.5$ Hz. These coupling constants are in accordance with a predominant (+)-gauche orientation of hydroxyl groups $OH8^b$ and $OH7^b$. For unit c, no interglycosidic NOEs were observed, and therefore, an unambiguous assignment of protons $H8pro\text{-}R^c$ and $H8pro\text{-}S^c$ was not possible. All NOEs of **1** were positive at 310 K and 500 MHz. An expansion of the 2D NOESY spectrum is shown in Figure 2a. Seven interglycosidic NOEs were observed (Figure 2a): $H6^b-H4^c$, $H8pro\text{-}S^b-H4^c$, $H8pro\text{-}R^b-H4^c$, $H6^b-H3eq^c$, $H6^b-H3ax^c$, $H8pro\text{-}S^b-H3eq^c$, and $H8pro\text{-}R^b-H3eq^c$ (for stereoimages of **1**, cf. Figure 7). This is unusual for glycosidic linkages where usually not more than one or two such NOEs are found. In a previous study (*33*), only one out of these seven interglycosidic NOEs, namely, the NOE $H6^b-H3eq^c$, was reported, probably because no detailed conformational analysis was intended. Metropolis Monte Carlo (MMC) simulations with a temperature parameter of 2000 K were chosen to allow sampling of the whole conformational space that is sterically accessible to **1** (*13*). Contour plots of the conformer distribution around the glycosidic linkage in **1** are shown in panels a and b of Figure 4, with the position of the global minimum A and a local minimum B indicated. In both MMC simulations, the side chains of the pyranose rings exhibited high flexibility. No extra torsional potentials were applied to the C6−C7 and the C7−C8 bonds. A

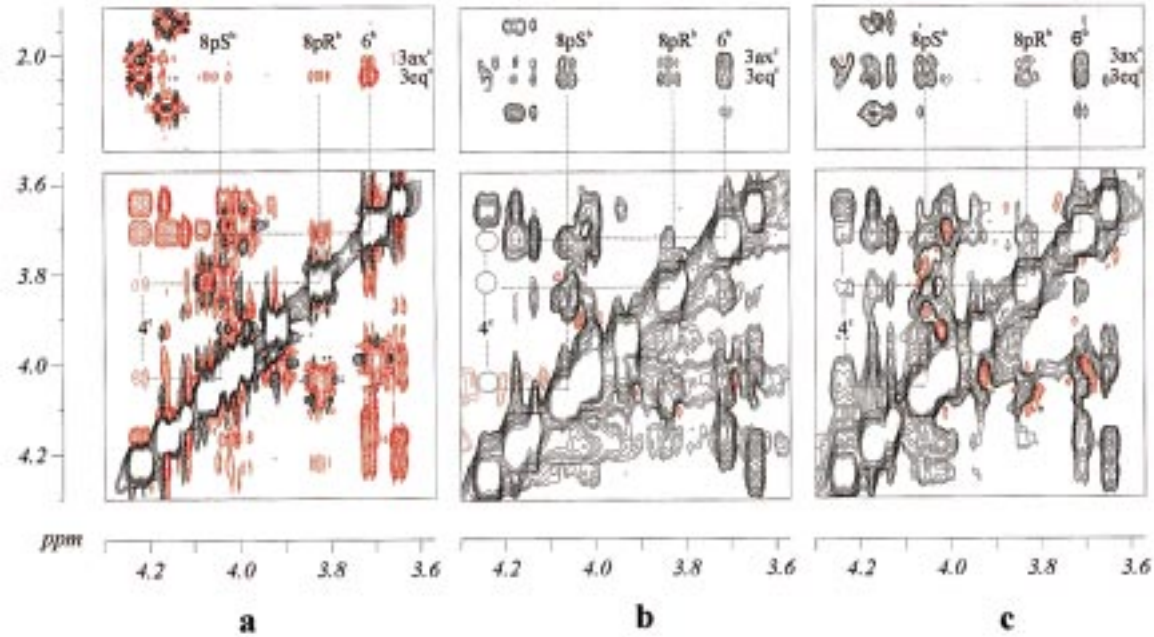

FIGURE 2: 2D NOESY and 2D trNOESY spectra of **1** (310 K, 500 MHz): (a) aqueous solution, (b) in the presence of mAb S25-2, and (c) in the presence of mAb S23-24. Mixing times were (a) 900, (b) 150, and (c) 150 ms. Positive contours are red, and negative contours are black.

Table 3: Upper and Lower Distance Constraints for α-Kdo-(2→4)-α-Kdo-(2→O)-allyl **1** Complexed with S25-2[a]

	disaccharide **1**−S25-2	
	lower distance (Å)	upper distance (Å)
positive constraints		
$H6^b-H3ax^c$	2.28	3.43
$H6^b-H3eq^c$	2.43	3.65
$H8pro\text{-}R^b-H3ax^c$	2.69	4.04
$H8pro\text{-}R^b-H3eq^c$	2.70	4.05
$H8pro\text{-}S^b-H3ax^c$	2.56	3.85
$H8pro\text{-}S^b-H3eq^c$	2.61	3.92
negative constraints		
$H4^c-H6^b$	3.50	−
$H4^c-H8pro\text{-}S^b$	3.50	−
$H4^c-H8pro\text{-}R^b$	3.50	−

[a] All values were derived from trNOE buildup curves as described in the text. Positive constraints result from trNOEs that have been observed. Negative constraints result from trNOEs that were absent.

Table 4: Relative NOEs and trNOEs (Percentage) from NMR Experiments and MMC Calculations[a]

proton−proton contact	exptl NOEs in aqueous solution	MMC simulation	exptl trNOEs with S25-2	exptl trNOEs with S23-24
$H4^c-H6^b$	47.0	36.5	−	44.8
$H4^c-H8pro\text{-}R^b$	18.0	4.7	−	33.0
$H4^c-H8pro\text{-}S^b$	24.3	3.6	−	120.9
$H3eq^c-H6^b$	52.0	91.5	49.1	72.8
$H3eq^c-H8pro\text{-}R^b$	9.6	2.8	40.6	54.3
$H3eq^c-H8pro\text{-}S^b$	8.3	2.2	50.8	49.56
$H3ax^c-H6^b$	12.6	7.4	55.9	40.80
$H3ax^c-H8pro\text{-}R^b$	−	0.2	32.8	44.9
$H3ax^c-H8pro\text{-}S^b$	−	0.2	35.7	63.4

[a] All values are relative to the intraglycosidic $H4^c-H6^c$ NOE (100%). All experiments were performed at 310 K. In aqueous solution, the mixing time was 900 ms. trNOEs were determined from a trNOESY spectrum with a mixing time of 250 ms. For the MMC simulation, the mixing time was set to 900 ms, and the temperature parameter was set to 600 K. The correlation time was 150 ps (*13*).

comparison between theoretical NOEs calculated from either minimum A or minimum B clearly did not fit the experimental data. For instance, no interglycosidic NOEs between $H6^b$ and $H4^c$ would be expected in minimum B. On the other hand, neither would NOEs between the side chain protons H8 in ring b and the deoxy proton H3eq in ring c be predicted for minimum A, or closely related conformers, nor would an NOE between $H6^b$ and $H3ax^c$ be observed. Therefore, ensemble average NOEs were calculated from a MMC calculation at 600 K (*34*) and compared to experimental NOEs. From Table 4, it is seen that the gross conformational properties of **1** are reproduced by the simulation. Even the interglycosidic NOE contacts to the side chain protons H8 in ring b are correctly predicted on a qualitative level. The quantitative comparison of experimental and theoretical NOEs reveals deviations, showing that the approximations that have been made do not permit a precise description of the conformational behavior of disaccharide **1** in aqueous solution. Therefore, we conclude that the conformational properties of disaccharide **1** in aqueous solution are described well by a model where two major conformational families are present. One of the families is characterized by the global minimum A, and the other family is represented by the local minimum B. The dihedral angles (ϕ and ψ) at the (2→4)-glycosidic linkage for minimum A and minimum B are −78° and −26°, and −52° and 5°, respectively. From the population plots in Figure 4, it is apparent that the ψ angle spans a larger range than the ϕ angle, a property that is important if one analyzes possible bound conformations. Furthermore, the MMC simulation with a temperature parameter of 2000 K shows an additional minimum D (Figure 4b). Conformers corresponding to minimum D would lead to the observation of a strong interglycosidic NOE between $H4^c$ and $H3eq^b$ (∼2.5 Å) and a weak effect between $H4^c$ and $H3ax^b$ (∼3.8 Å). Since none of these two interglycosidic NOEs was detected, a significant population of the region around minimum D is unlikely, although the presence of small amounts of D cannot totally be excluded. Stereoimages of minima A and B are shown in Figure 7. Dihedral angles and relative energies of energy minima A−D are summarized in Table 5.

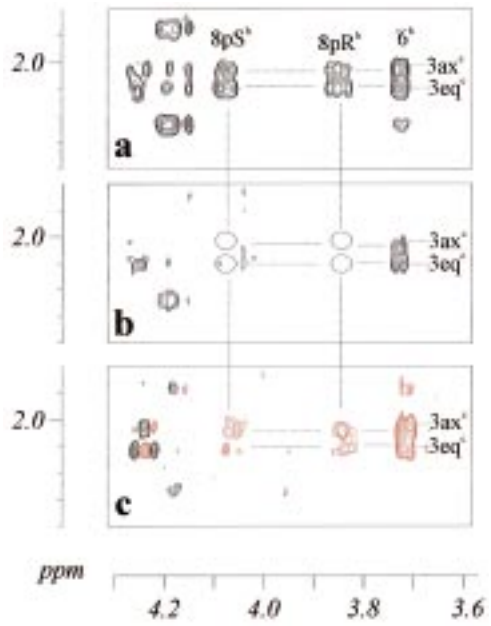

FIGURE 3: Parts of 2D trNOESY (a), 2D trROESY (b), and 2D QUIET-trNOESY (c) spectra of **1** bound to S25-2. The QUIET-trNOESY experiment was carried out with a 15 ms double-band selective Q3 inversion pulse (inversion of regions 4.10−3.60 and 2.17−1.67 ppm). Peaks within the inverted regions exhibit an opposite sign (red) relative to the other cross-peaks outside these regions. The mixing time was 250 ms for all experiments. A comparison of the spectra allows identification of spin diffusion effects. Cross-peaks that are canceled in the trROESY spectrum because spin diffusion and direct dipolar interactions take place at the same time (see the discussion in the text) are marked with circles in the 2D trROESY spectrum (Figure 2b).

Binding Affinities of mAbs. Binding of monoclonal antibodies was tested in an EIA system using synthetic neoglycoconjugates as solid phase antigens. The results are shown in Figure 5. Whereas mAb S25-2 bound to the homologous antigen α-Kdo-(2→8)-α-Kdo-(2→O)-allyl **2** with a higher affinity (approximately 10-fold) than to the heterologous antigen α-Kdo-(2→4)-α-Kdo-(2→O)-allyl **1** (Figure 5, panels B and D), independent of whether high or low amounts of immobilized antigen were used, mAb S23-24 bound to the homologous and heterologous antigen at comparable antibody concentrations only when high amounts of antigen were used (400 pmol/mL, corresponding to 20 pmol/well). With low amounts of antigen (25 pmol/mL, corresponding to 1.25 pmol/well), similar binding to the homologous and heter-

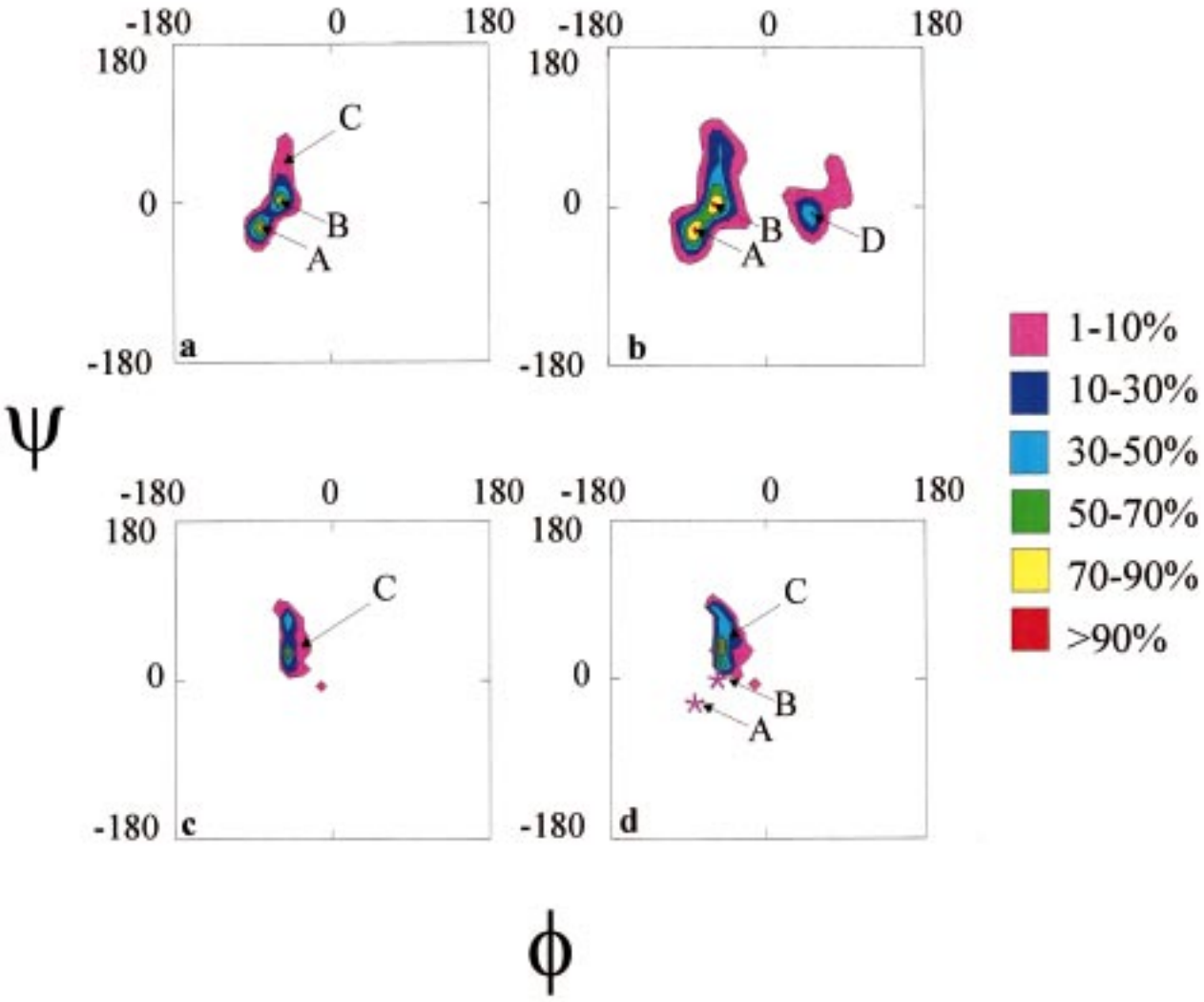

FIGURE 4: Contour plots showing the relative population of conformational space around the (2→4)-glycosidic linkage in **1**. The ϕ versus ψ maps were divided into bins of 10° in the ϕ and ψ directions, and the number of conformations in each bin was counted. Then, contour levels were calculated relative to the highest populated bin (global minimum). The contour levels are color-coded. Magenta represents 1−10%, dark blue 10−30%, light blue 30−50%, green 50−70%, yellow 70−90%, and red more than 90% of the number of conformations in the most populated bin. (a) MMC simulation at 600 K. (b) MMC simulation at 2000 K. (c and d) Possible conformations of **1** bound to mAb S25-2. (c) All conformations from the MMC simulation at 2000 K that satisfy the positive distance constraints listed in Table 3 (0.15% of the total number of conformations from the MMC simulation). (d) All conformations that satisfy positive and negative distance constraints listed in Table 3 (0.075% of the total number of conformations).

Table 5: Dihedral Angles ϕ and ψ at the (2→4)-Glycosidic Linkage of **1** and the Corresponding Relative Energies of Minima A−D

	ϕ and ψ (deg)	relative energy (kcal/mol)		ϕ and ψ (deg)	relative energy (kcal/mol)
A	−78 and −26	0.0	C	−44 and 33	4.8
B	−52 and 5	0.2	D	62 and 8	3.2

ologous antigen required 20 times higher antibody concentrations for the hetrerologous antigen α-Kdo-(2→4)-α-Kdo-(2→O)-allyl **1** (Figure 5, panels A and C). No binding of the mAbs is observed for monosaccharide Kdo derivatives.

For the following discussion of trNOE experiments, it is important to compare the relative affinities of mAbs S25-2 and S23-24 for the synthetic antigen α-Kdo-(2→4)-α-Kdo-(2→O)-allyl **1**. Although no quantitative evaluation of binding affinities is possible from the EIA binding curves, relative affinities may be estimated. A comparison of antibody concentrations at an OD of 1.0 yields the dimension of relative binding affinities. Compared to S25-2, S23-24 binds to **1** with an about 50-fold higher affinity (Figure 5, panels A and B). This corresponds to a difference in the free energy of binding of about 2.4 kcal/mol. When the binding of the homologous antigen **2** and the binding of the heterologous antigen **1** to S25-2 are compared, a 10-fold higher affinity is estimated for **2**, corresponding to a difference in the free energy of binding of about 1.4 kcal/mol. A quantitative determination of binding constants is underway, and preliminary data support the qualitative results given here (*35*).

Analysis of the Bioactive Conformation of α*-Kdo-(2→4)-*α*-Kdo-(2→O)-allyl* ***1*** *Bound to mAb S25-2.* Upon binding to a receptor protein, flexible carbohydrate ligands usually are fixed in a specific bioactive conformation (*9*, *11*, *31*, *36*). In most cases, a conformation is bound that is also highly populated in solution, but cases have been reported in which high-energy conformers are stabilized upon binding to a protein (*9*, *10*, *12*), or where flexibility is conserved in the bound state because only a part of the molecule fits into the

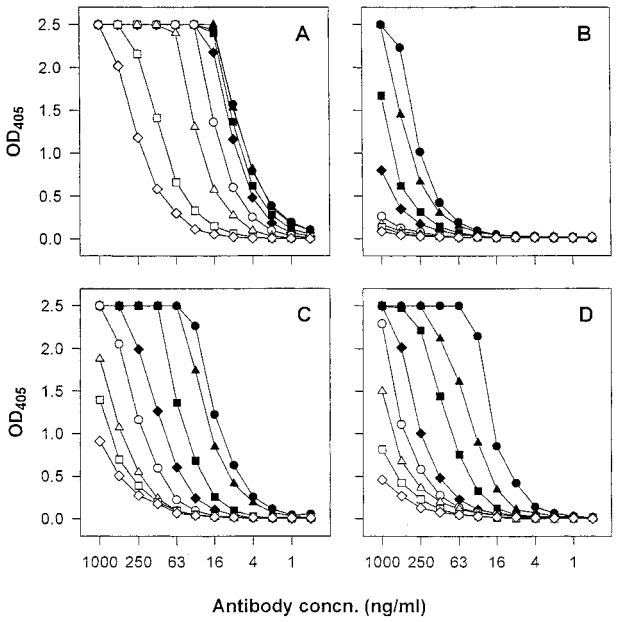

FIGURE 5: Binding curves (semilogarithmic) of monoclonal antibodies S23-24 (IgG_1) (A and C) and S25−2 (IgG_1) (B and D) against the Kdo disaccharides α-Kdo-(2→4)-α-Kdo-(2→O)-allyl (A and B) and α-Kdo-(2→8)-α-Kdo-(2→O)-allyl (C and D), representing partial structures of chlamydial LPS. EIA plates were coated with graded concentrations of neoglycoconjugates corresponding to 400 (●), 200 (▲), 100 (■), 50 (◆), 25 (○), 12.5 (△), 6.3 (□), and 3.2 (◇) pmol of ligand per mL using 50 μL per well and the mixtures reacted with monoclonal antibodies at the concentrations indicated on the abscissa. Values are the mean of quadruplicate determinations with confidence values not exceeding 10%.

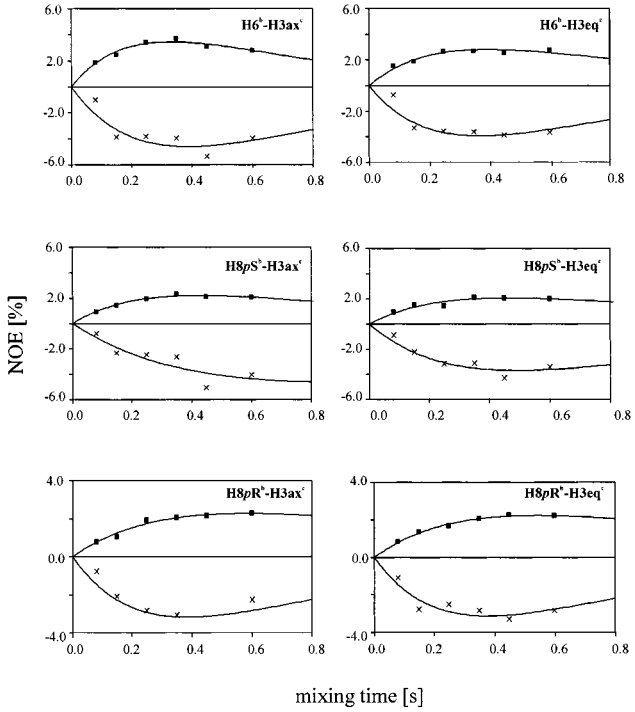

FIGURE 6: QUIET-trNOE (■) and corresponding trNOE (×) buildup curves of **1** bound to mAb S25-2. The NOEs were calculated as absolute values as described in the experimental part. Initial slopes and absolute NOEs are compared in Table 5.

binding pocket (*37*). As mentioned above, mAb S25-2 specifically recognizes **2**, and probably binds a conformer that is similar to the conformation also found in the crystal (*13*). Binding of S25-2 to **1** occurs with an affinity that is reduced by approximately 2 orders of magnitude, raising the interesting question of which of the conformers of **1** presented to the antibody in solution will be recognized and bound.

Addition of S25-2 to an aqueous solution of **1** leads to the observation of strong negative trNOEs. The trNOESY spectrum of disaccharide **1** in the presence of mAb S25-2 exhibits a significantly different trNOESY cross-peak pattern (Figure 2b) compared to the NOESY spectrum of **1** in aqueous solution (Figure 2a). In the trNOESY experiment, additional cross-peaks indicating short distances between proton pairs $H3ax^c$−$H8pro\text{-}R^b$ and $H3ax^c$−$H8pro\text{-}S^b$ are observed. Most remarkable is the disappearance of an interglycosidic NOE between protons $H4^c$ and $H6^b$ that is predominant for **1** in aqueous solution (Figure 2, panels a and b). Also, the weak interglycosidic NOEs between $H4^c$ and protons $H8pro\text{-}R^b$ and $H8pro\text{-}S^b$ disappear. From these observations alone, it is clear that the global minimum A is not bound by S25-2, since a strong or at least moderate trNOE between $H4^c$ and $H6^b$ would be expected.

Also, the trNOE cross-peak pattern is not consistent with local minimum B bound by the antibody. No orientation of the side chain in ring b can be found where interglycosidic trNOEs between protons $H8pro\text{-}R^b$ and $H8pro\text{-}S^b$ and $H3ax^c$ are predicted. Since it is well-documented that especially in trNOE experiments spin diffusion effects can lead to false distance constraints (*12*, *24*, *38*), we performed trROESY experiments to verify the observed trNOEs. Figure 3 shows corresponding regions of a trNOESY (Figure 3a) and a trROESY (Figure 3b) spectrum. No trROEs between the protons attached to $C8^b$ and those bound to $C3^c$ were observed. This observation would be compatible with a conformation related to minimum B bound by mAb S25-2, with the side chain of residue b oriented such that no dipolar contacts occur across the glycosidic linkage of **1**. In the following, we will show that this conclusion is wrong and, in general, that the acquisition of a trNOESY experiment in conjunction with a trROESY experiment is not sufficient to unambiguously rule out spin diffusion.

One drawback of the trROESY experiment is that no sign discrimination is possible, and therefore, cross-peaks could be due either to ROEs or to trROEs. For instance, in the trROESY spectrum, a cross-peak between $H4^c$ and $H6^b$ is observed, stemming from the dipolar interaction of the two protons in the free state of **1**. On the other hand, it is well possible that spin diffusion processes and direct dipolar interactions occur at the same time, leading to cancellation of the positive contributions from direct dipolar contacts and the negative contributions from spin diffusion. Therefore, we carried out several NMR experiments that are capable of separating spin diffusion from direct dipolar interactions. One class of experiments, termed MINSY experiments (*26*), allowed us to selectively switch off relaxation pathways during the mixing time of a (tr)NOESY experiment by selectively saturating a spin or a group of spins that are suspected to participate in spin diffusion pathways. Clearly, in our case, spin diffusion might occur between protons $H3ax^c$ and $H3eq^c$ (Figure 7) since they are very close in space. Therefore, we carried out 1D MINSY experiments, i.e., 1D transient NOE experiments with saturation of certain resonances during the mixing time. First, we selectively

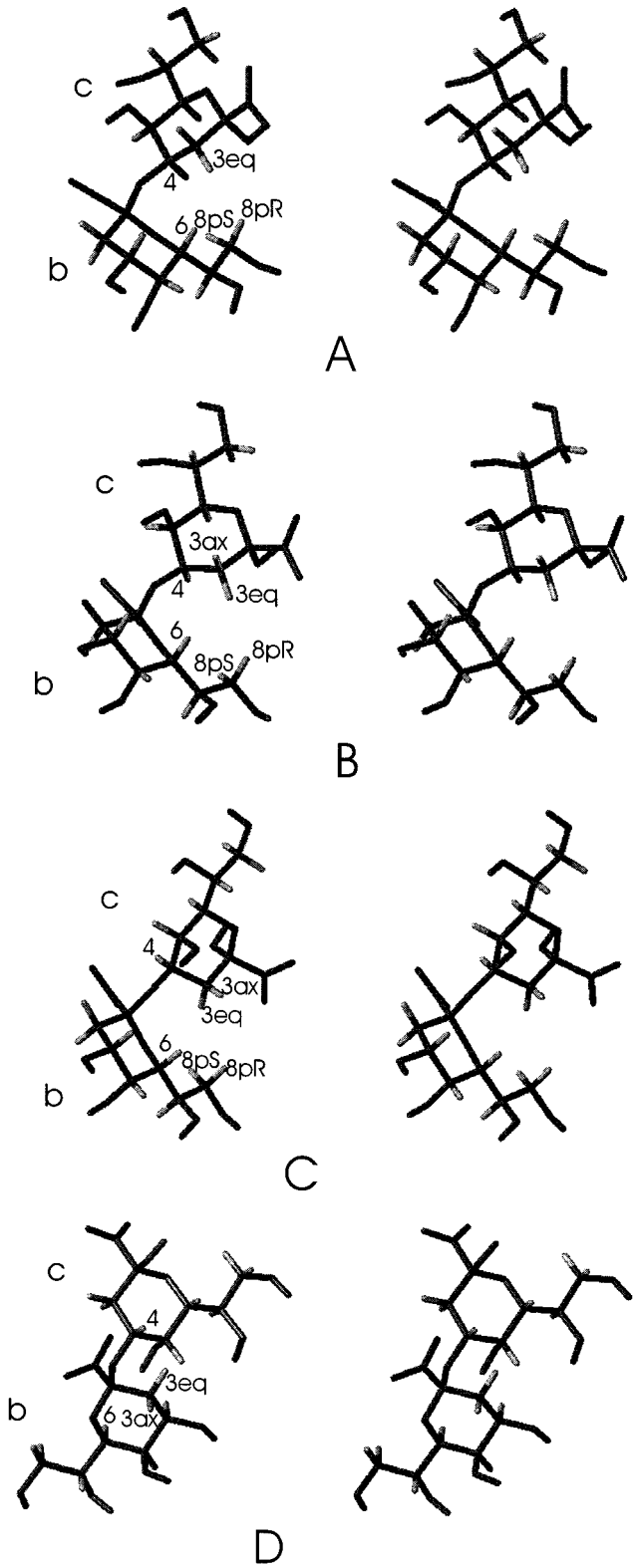

FIGURE 7: Stereoimages of **1** (relaxed view): (A) global minimum A, (B) local minimum B, (C) conformation C that is recognized by mAb S25-2, and (D) local minimum D.

inverted H3eq^c, and during the mixing time, we saturated H3ax^c with low-power rf. All interglycosidic trNOEs that were observed in the 2D trNOESY experiment are still present, and in particular, no intensity changes were found for the interglycosidic trNOE between H3eq^c and H6^b. Second, we inverted H3ax^c and saturated H3eq^c during the mixing time. Again, the same interglycosidic trNOEs as in the 2D trNOESY spectrum were observed. Thus, it is highly unlikely that the protons attached to C3^c participate in spin diffusion processes. Another explanation for the occurrence of spin diffusion-mediated trNOEs from the protons at C3^c to the protons bound to C8^b would be spin diffusion via H6^b as a relay spin. 1D MINSY experiments where H6^b was selectively saturated during the mixing time clearly showed that this is not the case. Therefore, we conclude that protons attached to disaccharide ligand **1** are not likely to contribute much to any spin diffusion pathway. This is explained by the fact that with the large excess of ligand molecules used in trNOE experiments the fraction of protein complexed with ligand is close to 1. It follows that the transfer of magnetization from a ligand proton to a protein proton is more efficient than to a proton at the same distance within the ligand. This renders spin diffusion via protein protons more efficient than via ligand protons. The topic has been discussed in detail by Ni and Zhu (*39*), Moseley et al. (*2*), Arepalli et al. (*38*), and Vincent et al. (*24*). To summarize, protein protons are the major source of spin diffusion.

To test this hypothesis, we carried out a class of recently developed NMR experiments, namely QUIET-(tr)NOESY experiments (*24*, *40*). These experiments work by an "inverse MINSY principle"; i.e., instead of relay spins during the mixing time being silenced via saturation, pairs or groups of spins between which (tr)NOEs are expected are inverted with a double or multiple selective shaped 180° pulse at the center of the mixing period leading to a cancellation of all magnetization transfers, except the ones that are due to direct dipolar interactions between the spins of interest.

We performed four QUIET-trNOESY experiments employing different multiple selective inversion pulses. In one QUIET-trNOESY experiment, in the following referred to as experiment 1, protons in the range between 4.12 and 3.80 ppm (this region encompasses protons H8*pro-R*^{b} and H8*pro-S*^{b}) and between 2.30 and 1.98 ppm (protons H3ax^c and H3eq^c) were inverted with a double selective 180° Gaussian Q3 pulse cascade (*25*). In this experiment, proton H6^b is excluded as a source of spin diffusion. In another QUIET-trNOESY experiment, in the following referred to as experiment 2, the spectral regions encompassing protons H8*pro-R*^{b} and H6^b (3.92−3.60 ppm) and protons H3ax^c and H3eq^c (2.30−1.98 ppm) were inverted with a double selective 180° Gaussian Q3 pulse cascade (*25*). The purpose was to exclude H8*pro-S*^{b} as a possible relay spin for spin diffusion. In a triple inversion QUIET-trNOESY experiment, in the following referred to as experiment 3, protons H8*pro-S*^{b} (4.32−4.00 ppm), H6^b (3.80−3.48 ppm), and H3ax^c and H3eq^c (2.30−1.98 ppm) were selectively inverted. In this experiment, proton H8*pro-R*^{b} was excluded as a possible source of spin diffusion within the ligand. Experiment 4 (results from this experiment are shown as a representative example in Figure 3c) was a QUIET-trNOESY experiment where all protons between 4.1 and 3.60 ppm and between 2.17 and 1.67 ppm were inverted by applying a band selective inversion pulse.

In experiment 1, trNOEs H8*pro-S*^{b}−H3ax^c, H8*pro-R*^{b}−H3ax^c, H8*pro-S*^{b}−H3eq^c, and H8*pro-R*^{b}−H3eq^c were observed. Experiment 2 produced interglycosidic trNOEs H8*pro-R*^{b}−H3ax^c, and H8*pro-R*^{b}−H3eq^c. Experiment 3 led to the observation of trNOEs H8*pro-S*^{b}−H3ax^c and H8*pro-S*^{b}−H3eq^c. In experiment 4 (Figure 3c), all of the above-

Table 6: Comparison of QUIET-trNOESY and trNOESY Data[a]

	attenuation factor *k*		
proton pair	initial slope	$\tau_{mix} = 20$ ms	$\tau_{mix} = 450$ ms
H6[b]−H3ax[c]	0.88	0.87	0.72
H6[b]−H3eq[c]	0.66	0.68	0.73
H8*pro*-*S*[b]−H3ax[c]	0.93	0.91	0.56
H8*pro*-*S*[b]−H3eq[c]	0.61	0.61	0.56
H8*pro*-*R*[b]−H3ax[c]	0.48	0.48	0.70
H8*pro*-*R*[b]−H3eq[c]	0.50	0.51	0.71

[a] Attenuation factors *k* were obtained by dividing the initial slopes (or intensities) of the QUIET-trNOESY curves shown in Figure 6 by the corresponding values of the trNOESY curves. The values at mixing times of 20 and 450 ms were taken from fitted curves.

mentioned trNOEs were observed. A qualitative comparison shows that the trNOE patterns in experiments 1−4 are very similar. It follows that spins H6[b] (experiment 1), H8*pro*-*S*[b] (experiment 2), and H8*pro*-*R*[b] (experiment 3) are not the source of spin diffusion processes. All QUIET-trNOESY experiments described above suppress spin diffusion via aromatic, and largely also via aliphatic, protein protons.

For a quantitative evaluation, the setup of experiment 4 (Figure 3c) was chosen because this experiment allows an analysis of all relevant trNOE curves at the same time. TrNOE buildup curves were obtained and compared to buildup curves from normal trNOESY experiments. Curves for prominent interglycosidic trNOEs are shown in Figure 6. First, it is observed that all trNOEs from 2D QUIET-trNOESY experiments are smaller than the corresponding effects from trNOESY experiments. A constant portion of this attenuation is due to unavoidable losses of magnetization through longitudinal and transversal relaxation processes during the band selective inversion pulse, and through rf inhomogeneities of this pulse. This has been described in detail by Zwahlen et al. (*40*), where an overall attenuation factor between 0.7 and 0.9 is discussed. No attempt was made to separate spin diffusion contributions from this overall attenuation. Nevertheless, the relative changes between the two sets of buildup curves may be compared. Therefore, in Table 6, we compare initial slopes obtained from trNOESY buildup curves to those from QUIET-trNOESY buildup curves. In addition, we supply a comparison of trNOEs at mixing times of 20 and 450 ms. The factors *k* compiled in Table 6 are the attenuation factors between trNOESY and QUIET-trNOESY experiments. It is obvious that the attenuation factors *k* for the initial slopes or for trNOEs with a very short mixing time of 20 ms differ by up to a factor of 2. It follows that not taking into account spin diffusion can introduce significant errors in determining distance constraints (*24*). With longer mixing times, the influence of spin diffusion is increasing, and therefore, it is not surprising that attenuation factors are quite different for trNOEs obtained with a mixing time of 450 ms.

Interproton distances were derived from the initial slopes of the QUIET-trNOESY buildup curves using the isolated spin pair approximation. Then, upper and lower distance constraints were derived from the distances by adding ±20% to the distances that were derived. All distance constraints that were used are summarized in Table 3, where negative constraints are due to trNOEs that were not observed. To obtain bound conformations that fulfill the constraints of Table 3, a MMC simulation with 2×10^6 steps was performed at 2000 K (*13*, *31*). The high-temperature parameter allows efficient sampling of the conformational space that is available to disaccharide **1** as this is recognized from Figure 4 where the results of MMC simulations at 600 K (Figure 4a) and at 2000 K (Figure 4b) are shown as population plots. Contour lines are color-coded and give the proportion of conformers relative to the area with the highest population. It is obvious that the local minimum D is only sampled if the temperature parameter is set to 2000 K. The dihedral angles at the (2→4)-glycosidic linkage and the relative energies of minima A−D are summarized in Table 5, with the corresponding stereodrawings in Figure 7. From the 2000 K MMC simulation, an ensemble of 1.3×10^6 conformations was obtained (Figure 4b). In a first step, all conformations that satisfied the positive distance constraints in Table 3 were selected, yielding 2×10^3 (0.15% of all conformations derived from MMC) conformations. The resulting population of conformations is shown in the contour plot in Figure 4c, demonstrating that the positive constraints already significantly reduce the number of possible bound conformations. In general, the use of negative distance constraints is critical because the absence of NOEs is attributed entirely to the geometry of the molecule. Therefore, we use the negative constraints in Table 3 only to support the range of possible bound conformations. In Figure 4d is shown a contour plot that corresponds to those conformations that satisfy both positive and negative constraints in Table 3 (1×10^3 conformations, 0.075%). It is obvious that the inclusion of negative constraints does not lead to a significant reduction of the number of possible bound conformations. On the other hand, the inclusion of negative constraints is not in conflict with the results derived exclusively from positive constraints. It follows that the absence of the corresponding trNOEs is most likely due to geometrical reasons.

The ensemble of possible bound conformations (Figure 4, panels c and d) reflects the experimental accuracy with which the bioactive conformation of **1** can be described. It is obvious that the bioactive conformation lies in a range of the energy surface of the (2→4)-glycosidic linkage that is not highly populated in aqueous solution. In Figure 7, we show a stereoimage of conformation C that represents the bioactive conformation of **1**. This conformation is clearly distinct from the global minimum A but differs from the local minimum B only by an alteration of the ψ angle (cf. Table 5).

It is concluded that upon binding of **1** to S25-2 a conformation C (Figure 7), or a similar structure (Figure 4, panels c and d), is selected that is not populated to a detectable (by NMR) amount in aqueous solution.

Analysis of the Bioactive Conformation of α*-Kdo-(2→4)-*α*-Kdo-(2→O)-allyl* ***1*** *Bound to mAb S23-24.* NMR studies of the recognition reaction between mAb S23-24 that preferentially binds to a (2→4)-glycosidic linkage between Kdo monomers were performed in analogy to the studies explained in detail above. First, trNOESY spectra of disaccharide **1** in the presence of S24-23 were recorded (Figure 2c). It is obvious that the pattern of trNOE cross-peaks is similar to the pattern of NOE cross-peaks of disaccharide **1** in aqueous solution. The interglycosidic trNOE between protons H6[b] and H4[c] is especially present. From this observation alone, it is clear that a conformation of **1** is bound

by S23-24 that is closely related to minimum A, which is highly populated in aqueous solution.

For the analysis of the bioactive conformation of **1** when it is bound to mAb S23-24, a band selective QUIET-trNOESY spectrum was acquired. From the experimental trNOEs, possible bound conformations were derived, essentially using the same strategy outlined above for the complex of **1** with S25-2. Interestingly, in addition to the interglycosidic trNOE between $H6^b$ and $H4^c$ trNOEs, interglycosidic trNOEs H8*pro-S*^{b}−H3ax^c, H8*pro-R*^{b}−H3ax^c, H8*pro-S*^{b}−H3eq^c, and H8*pro-R*^{b}−H3eq^c were observed in the trNOESY as well as in the QUIET-trNOESY spectra. trNOEs were translated into distance constraints between 2.00 and 3.50 Å (Table 3) as described above, but these upper and lower distance constraints resulted in no possible solution. The major problem is that none of the side chain conformations of ring b can give rise to interglycosidic trNOEs H8*pro-S*^{b}−H3ax^c and H8*pro-R*^{b}−H3ax^c if at the same time a trNOE indicates a short distance between $H6^b$ and $H4^c$.

Therefore, we conclude that mAb S23-24 recognizes different conformations of **1**. One bound conformation clearly is very similar to minimum A since a trNOE between $H6^b$ and $H4^c$ was observed. From the discussion of the conformation of **1** bound to S25-2, it is also clear that conformation C (Figure 7) is bound, too. For C, trNOEs from protons H8*pro-S*^{b} and H8*pro-R*^{b} to both protons at $C3^c$, $H3eq^c$ and $H3ax^c$, are expected (for B, only dipolar contacts to $H3eq^c$ are possible), as observed. This shows that at least two conformations, A and C, of **1** are recognized by mAb S23-24. Since the presumption of a single bound conformation is no longer valid, minimum B cannot be ruled out as a bound conformation, too, and all trNOEs must be understood as average values from different conformers. This makes a quantitative interpretation of trNOEs very complicated, and no attempt was made to solve this problem.

CONCLUSIONS

We have demonstrated that a correct interpretation of trNOEs requires a careful experimental examination of spin diffusion pathways. If only trROESY experiments were used to identify spin diffusion, four out of six positive distance constraints would have been unusable. TrROESY experiments alone are not sufficient, if magnetization transfer results from spin diffusion and direct dipolar interactions at the same time. Opposite signs of the related cross-peaks may lead to cancellation, or significant attenuation, and as a result, corresponding distance constraints would furnish false models for the bound conformation of a ligand. The application of QUIET-trNOESY experiments (*24*, *40*) efficiently suppresses effects resulting from spin diffusion without leading to cancellation. It has been argued previously that spin diffusion mediated by protein protons is a major source of error (*2*, *24*, *38*, *39*). Experiments performed in this study strongly support this finding, and therefore, we suggest the application of band selective QUIET-trNOESY experiments with selective inversion of all ligand resonances as a general strategy.

From trNOE data that have been corrected for spin diffusion in the above-mentioned manner, we concluded that mAbs S25-2 and S23-24 recognize one conformation of **1** that belongs to a family of conformers around minimum C. This minimum is not highly populated in aqueous solution. In addition, S23-24 binds to a conformation that is very similar to global minimum A. Distinct binding modes of carbohydrates have been described previously in the case of an H-type II trisaccharide binding to three different lectins (*41*), and it is quite reasonable that flexible ligands such as carbohydrates may be bound in different conformations. A recently published study describes a large conformational change of a pentasaccharide bound to a monoclonal antibody for one monosaccharide residue that lies outside the formal antibody binding site without changing the primary recognition unit (*10*). In comparison, in our investigation it is observed that conformational changes upon binding may also occur inside this primary recognition unit.

A final remark should be made with regard to the precision that is possible for the determination of a bound conformation using the approach described. The range of conformations of **1** that may be bound by S25-2 expands into areas of conformational space that are close to minimum B (Figure 4, panels c and d). Whereas conformation C is ca. 4.8 kcal/mol above the global minimum A (Table 5), conformations with smaller ψ angles have lower relative conformational energies (Figure 4, panels a and b). For instance, conformation C′ ($\phi = -44°$, $\psi = 15°$) that is well within the range of possible bound conformations (Figure 4, panels c and d) has a relative energy that is 2.7 kcal/mol above the global minimum A. Such a value would be in agreement with the estimated reduction of 2.4 kcal/mol in the free energy of binding for binding of S25-2 to disaccharide **1** as compared to that for the binding of S23-24 to **1**. Whether it is really conformation C or C′ that is bound by the mAb cannot be determined by our current experimental data. To summarize, the range of possible bound conformations (to S25-2) of **1** given in panels c and d of Figure 4 reflects the precision with which the bioactive conformation of **1** can be described.

It may be hypothesized that mAb S25-2 recognizes a different epitope (governed mainly by disaccharide **2**) than S23-24, leading to a distinct mode of binding for heterologous antigen **1**. A comparison of the bound conformations of disaccharides **1** and **2** is difficult, mainly because a rather large range of possible bound conformations had been identified for **2** (*13*). Attempts to compare the crystal structure conformation of **2** with bound (to S25-2) conformation C of **1** show that it is impossible to achieve a satisfying match of the two conformers. Nevertheless, it may be reasonable to assume that a portion of residue c in **1** partially mimics residue b in **2**.

Currently, we are performing further NMR experiments to obtain a more precise epitope mapping of **1** and related carbohydrate ligands. Also, we are extending our studies to a variety of other mAbs with different specificities to obtain a more complete picture of the fine specificities of binding.

SUPPORTING INFORMATION AVAILABLE

Pulse sequence and pulse program (Bruker) used for the QUIET-trNOESY experiments. This material is available free of charge via the Internet at http://pubs.acs.org.

REFERENCES

1. Ni, F. (1994) *Prog. NMR Spectrosc. 26*, 517−606.
2. Moseley, H. N. B., Curto, E. V., and Krishna, N. R. (1995) *J. Magn. Reson., Ser. B 108*, 243−261.

3. Moseley, H. N. B., Lee, W., Arrowsmith, C. H., and Krishna, N. R. (1997) *Biochemistry 36*, 5239−5299.
4. Peters, T., and Pinto, B. M. (1996) *Curr. Opin. Struct. Biol. 6*, 710−720.
5. Poveda, A., and Jiménez-Barbero, J. (1998) *Chem. Soc. Rev. 27*, 133−143.
6. Meyer, B., Weimar, T., and Peters, T. (1997) *Eur. J. Biochem. 246*, 705−709.
7. Peters, T., and Meyer, B. (1997) German Patent 19649359 (international patent pending).
8. Henrichsen, D., Ernst, B., Magnani, J. L., Wang, W.-T., Meyer, B., and Peters, T. (1999) *Angew. Chem., Int. Ed. 38*, 98−102.
9. Espinosa, J. F., Montero, E., Vian, A., García, J. L., Dietrich, H., Schmidt, R. R., Martín-Lomas, M., Imberty, A., Canada, F. J., and Jiménez-Barbero, J. (1998) *J. Am. Chem. Soc. 120*, 1309−1318.
10. Milton, M. J., and Bundle, D. R. (1998) *J. Am. Chem. Soc. 120*, 10547−10548.
11. Bundle, D. R., Baumann, H., Brisson, J.-R., Gagne, S. M., Zdanov, A., and Cygler, M. (1994) *Biochemistry 33*, 5183−5192.
12. Weimar, T., Harris, S. L., Pitner, J. B., Bock, K., and Pinto, B. M. (1995) *Biochemistry 34*, 13672−13680.
13. Sokolowski, T., Haselhorst, T., Scheffler, K., Weisemann, R., Kosma, P., Brade, H., Brade, L., and Peters, T. (1998) *J. Biomol. NMR 12*, 123−133.
14. Rietschel, E. T., Kirikae, T., Schade, F. U., Mamat, U., Schmidt, G., Loppnow, H., Ulmer, A. J., Zähringer, U., Seydel, U., and Di Padova, F. (1994) *FASEB J. 8*, 217−225.
15. Brade, L., Kosma, P., Appelmelk, B. J., Paulsen, H., and Brade, H. (1987) *Infect. Immun. 55*, 462−466.
16. Fu, Y., Baumann, M., Kosma, P., Brade, L., and Brade, H. (1992) *Infect. Immun. 60*, 1314−1321.
17. Mikol, V., Kosma, P., and Brade, H. (1994) *Carbohydr. Res. 263*, 35−42.
18. Kosma, P., Gass, J., Schulz, G., Christian, R., and Unger, F. M. (1987) *Carbohydr. Res. 167*, 39−54.
19. Brade, L., Zych, K., Rozalski, A., Kosma, P., Bock, K., and Brade, H. (1997) *Glycobiology 7*, 819−827.
20. Lowry, O. H., Rosebrough, N. J., Farr, A. L., and Randall, R. L. (1951) *J. Biol. Chem. 193*, 265−275.
21. Marion, D., and Wüthrich, K. (1983) *Biochem. Biophys. Res. Commun. 113*, 967−974.
22. Hwang, T.-L., and Shaka, A. J. (1992) *J. Am. Chem. Soc. 114*, 3157−3159.
23. Scherf, T., and Anglister, J. (1993) *Biophys. J. 64*, 754−761.
24. Vincent, S. J. F., Zwahlen, C., Post, C. B., Burgner, J. W., and Bodenhausen, G. (1997) *Proc. Natl. Acad. Sci. U.S.A. 94*, 4383−4388.
25. Emsley, L., and Bodenhausen, G. (1992) *J. Magn. Reson. 97*, 135−148.
26. Massefski, W., and Redfield, A. G. (1988) *J. Magn. Reson. 78*, 150−155.
27. Neidig, K.-P., Geyer, M., Görler, A., Antz, C., Saffrich, R., Beneicke, W., and Kalbitzer, R. (1995) *J. Biomol. NMR 6*, 255−270.
28. Stuike-Prill, R., and Meyer, B. (1990) *Eur. J. Biochem. 194*, 903−919.
29. Peters, T., Meyer, B., Stuike-Prill, R., Somorjai, R., and Brisson, J.-R. (1993) *Carbohydr. Res. 238*, 49−73.
30. Meyer, B., Zsiska, M., and Stuike-Prill, R. (1993) in *Computer Simulations Studies in Condensed Matter Physics IV* (Landau, D. P., Mon, K. K., and Schuttler, H. B., Eds.) pp 90−112, Springer-Verlag, Berlin.
31. Scheffler, K., Ernst, B., Katopodis, A., Magnani, J. L., Wang, W. T., Weisemann, R., and Peters, T. (1995) *Angew. Chem., Int. Ed. 34*, 1841−1844.
32. Weimar, T., Peters, T., Pérez, S., and Imberty, A. (1997) *THEOCHEM 395/396*, 297−311.
33. Bock, K., Thomsen, J. U., Kosma, P., Christian, R., Holst, O., and Brade, H. (1992) *Carbohydr. Res. 229*, 213−224.
34. Peters, T., and Weimar, T. (1994) *J. Biomol. NMR 4*, 97−116.
35. Müller-Lönnies, S., MacKenzie, C. R., Patenaude, S. I., Evans, S. V., Kosma, P., Brade, H., Brade, L., and Narang, S. (1999) *Eur. J. Biochem.* (submitted for publication).
36. Bevilacqua, V. L., Yangmee, K., and Prestegard, J. H. (1992) *Biochemistry 31*, 9339−9349.
37. Weimar, T., and Peters, T. (1994) *Angew. Chem., Int. Ed. 33*, 88−91.
38. Arepalli, S. R., Glaudemans, C. P. J., Daves, G. D., Kovac, P., and Bax, A. (1995) *J. Magn. Reson., Ser. B 106*, 195−198.
39. Ni, F., and Zhu, Y. (1994) *J. Magn. Reson., Ser. B 102*, 180−184.
40. Zwahlen, C., Vincent, S. J. F., Di Bari, L., Levitt, M. H., and Bodenhausen, G. (1994) *J. Am. Chem. Soc. 116*, 362−368.
41. Du, M. H., Spohr, U., and Lemieux, R. U. (1994) *Glycoconjugate J. 11*, 443−461.

BI982984Z